Asian Journal of Pharmaceutical Sciences 16 (2021) 192–202

Available online at www.sciencedirect.com

ScienceDirect

journal homepage: www.elsevier.com/locate/AJPS

Original Research Paper

Gas-blasting nanocapsules to accelerate carboplatin lysosome release and nucleus delivery for prostate cancer treatment

Shunli Fu, Shuang Liang, Dandan Jiang, Rui Yang, Zipeng Zhang, Lili Chang, Xinke Zhang, Yongjun Liu, Na Zhang**

Department of Pharmaceutics, Key Laboratory of Chemical Biology (Ministry of Education), School of Pharmaceutical Sciences, Shandong University, Jinan 250012, China

ARTICLE INFO

Article history:
Received 30 March 2020
Revised 4 May 2020
Accepted 19 May 2020
Available online 20 June 2020

Keywords:
Carboplatin
Nanocapsule
pH-responsive release
Gas-blasting
Prostate cancer

ABSTRACT

To improve therapeutic effect and reduce severely side effects of carboplatin (CBP), the gas-generating nanocapsules were developed to accelerate CBP lysosome release and nucleus delivery. CBP/SB-NC was prepared by co-loading CBP and $NaHCO_3$ (SB) in nanocapsules using w/o/w emulsification solvent evaporation. They exhibited vesicle-like spherical morphology, uniform particle size and negative zeta potential. Reaching the tumor site with a relatively high concentration is the first step for CBP delivery and the results showed that CBP/SB-NC could effectively increase drug accumulation at tumor site. After that, the drug delivery carriers need to be internalized into tumor cells and the *in vitro* cellular uptake ability results showed CBP/SB-NC could be internalized into RM-1 cells more efficient than CBP solution. After internalized by RM-1 cells, the gas-blasting release process was tested in acid environment. It was demonstrated that 5 mg/ml $NaHCO_3$ was optimal to achieve pH-responsive gas-blasting release. *In vitro* release results showed that CBP significantly rapid release in acid environment (pH 5.0) compared to neutral pH (pH 7.4) ($P < 0.05$). Meanwhile, TEM and the change of the concentration of H^+ results exhibited that the explosion of CBP/SB_5-NC was more easily happened in lysosome acid environment (pH 5.0). The blasting release can accelerate CBP lysosome release to cytoplasm. Furthermore, the nucleus delivery results showed CBP/SB_5-NC can promote pH-triggered rapid nucleus delivery. And the results of Pt-DNA adduct assay showed that the binding efficiency between CBP and DNA of CBP/SB_5-NC was higher than CBP solution. At last, *in vitro* and *in vivo* anti-tumor efficacy proved that CBP/SB_5-NC could enhance anti-tumor activity for prostate cancer therapy. CBP/SB_5-NC also showed superior safety *in vitro* and *in vivo* by hemolysis assay and histopathological study. All of the results demonstrate that CBP/SB_5-NC would be an efficient gas-blasting release formulation to enhance prostate cancer treatment.

* Corresponding authors.
E-mail addresses: liuyongjun@sdu.edu.cn (Y.J. Liu), zhangnancy9@sdu.edu.cn (N. Zhang).
Peer review under responsibility of Shenyang Pharmaceutical University.

https://doi.org/10.1016/j.ajps.2020.05.002

1. Introduction

Prostate cancer ranks the second in the incidence of cancer in men (13.5%) and the fifth leading cause of cancer deaths worldwide (6.7%) [1,2]. Currently, the treatment of prostate cancer mainly includes radical prostatectomy, androgen deprivation therapy, chemotherapy, radiation therapy and immunotherapy [3–6]. Chemotherapy remains an indispensable systemic treatment for prostate cancer. It has advantages of showing therapeutic effect on both primary tumors and metastases, bring better clinical benefits to patients by eliminating residual tumor after operation, reducing tumor load, alleviating disease condition, controlling complications and improving quality of life [7].

Platinum (II) is one of the most important chemotherapeutic agents in prostate cancer treatment [8,9]. Carboplatin (CBP) is a second-generation platinum (II) compound which kills cancer cells by destroying DNA structure [10–12]. It was approved by the US FDA in 1989 and was recommended by treatment guidelines of NCCN (National Comprehensive Cancer Network) to treat prostate cancer [12–14]. However, the non-specific distribution of CBP causes severe side effects, including myelosuppression, neurotoxicity and ototoxicity, which greatly limit its clinical application [15–17].

To overcome this challenge, nanocarriers have shown great prospect in clinical to enhance therapeutic effect of chemotherapeutic agents [18–20]. Nanocarriers can increase tumor biodistribution of drug, prolong the survival rate, and reduce side effects. Especially, nanocarriers with stimuli-responsive release characteristics were developed to trigger the drug release in tumors, thus increase drug concentration in target tissue, and further enhance therapeutic efficiency [21]. Due to the good hydrophilicity, CBP was loaded by stimuli-responsive nanocarriers through chemical linkage in most studies. For example, we have coupled lauric acid (LA) and CBP to prepare CBP-LA micelles and glutathione (GSH)-mediated sensitive release was achieved [22]. Nuclear DNA is the main target of CBP, therefore effectively entering the nucleus is a key step for CBP. However, these simple stimuli-responsive nanocarriers did not show advantages in promoting nucleus delivery of CBP. In this study, we aimed to develop a physical encapsulated lysosome stimulate-sensitive release system. The accelerated lysosome release was expected to increase the intracellular concentration of CBP, thus promoting CBP to effectively enter the nucleus, which will further increase anti-tumor effect of CBP. Besides, this system holds potential to decrease the dosage, and reduces severely side effects during treatment.

To achieve our purpose, gas-blasting strategy nanocapsule was employed [23–25]. Since the pH of the tumor microenvironment (6.5–7.2) or lysosomes (5.0–6.0) are lower than that of normal tissues and blood (~7.4), HCO_3^- or CO_3^{2-} ($NaHCO_3$, NH_4HCO_3 and $CaCO_3$) can react with H^+ and release CO_2 bubble, which induced the blasting of nanocapsules and triggered CBP release [21,26,27]. In addition, gas-blasting strategy is quite suitable for the delivery and stimulus-responsive release of CBP. Both CBP and HCO_3^-/CO_3^{2-} are hydrophilic and can be simply co-loaded in the core of nanocapsules. After endocytosis to lysosomes, H^+ that infiltrated into nanocapsules from the acidic organelles would react with HCO_3^- or CO_3^{2-} to form CO_2 bubbles, which can accelerate CBP lysosome release, and thus to improve the anti-tumor effect of the CBP [21,28–30]. Because the tissues of mammals are immersed in an environment that usually contains HCO_3^-, and $NaHCO_3$ (SB) is the most commonly used buffer in standard cell culture media [31], therefore $NaHCO_3$ was selected as gas-blasting agents and co-loaded in the core of nanocapsules.

In this study, we developed $NaHCO_3$ and CBP co-loaded pH-responsive gas-blasting poly (lactic acid-polyethylene glycol) (PLA-PEG) nanocapsules (CBP/SB-NC) in order to increase the tumor accumulation of CBP and further improve the therapeutic selectivity and reduce side effects (Scheme 1). Nanocapsules have hydrophilic internal cavity structure ensuring a high encapsulation rate of CBP. This strategy holes advantages of simple preparation, avoidance of chemical reactions and specific response in lysosomes. Particle size, zeta potential, morphology, the optimal concentration of $NaHCO_3$ and pH-responsive release were characterized. Moreover, *in vitro* cytotoxicity activity, cellular uptake and pH-triggered rapid nucleus co-location were investigated on RM-1 cell. Then Pt-DNA adduct determination was further tested by ICP-MS. In addition, the *in vivo* imaging and anti-tumor study were carried out experimentally in RM-1-bearing prostate cancer murine model to evaluate the biodistribution and anti-tumor efficacy. In addition, primary safety evaluations were carried out. To the best of our knowledge, this is the first time that CBP and $NaHCO_3$ are co-loaded to achieve CBP CO_2-blasting release and nucleus delivery, providing the possibility to further improve the clinical application.

2. Materials and methods

2.1. Materials

Carboplatin (CBP) was purchased from Dalian Meilun Biotech Co., Ltd. (Dalian, China). Polylactic acid-Polyethylene glycol (PLA-PEG) was purchased from Shandong Academy of Pharmaceutical Science (Jinan, China). 3-(4, 5-Dimethylthiazol-2-yl)−2,5-diphenyltetrazolium bromide (MTT) was purchased from Solarbio (Shanghai, China). 1,1-dioctadecyl-3,3,3,3-tetramethylindotricarbocyanine iodide (DiR) was procured from Fanbo Biochemicals Co., Ltd (Beijing, China). Fluorescein isothiocyanate (FITC) was purchased from Sigma (MO, USA). DAPI was purchased from Sigma (USA). Doxorubicin hydrochloride (DOX•HCl) was purchased from Dalian Meilun Biotech Co., Ltd. (Dalian, China). Penicillin and streptomycin (1%), trypsin-EDTA (0.25%), phosphate and phosphate buffered saline (PBS) were the product of Solarbio Biotechnology Co. Ltd (Shanghai, China). Roswell Park Memorial Institute medium (RPMI-1640) were obtained from Hyclone. All materials and reagents used in this work were of analytical grade and used without further purification.

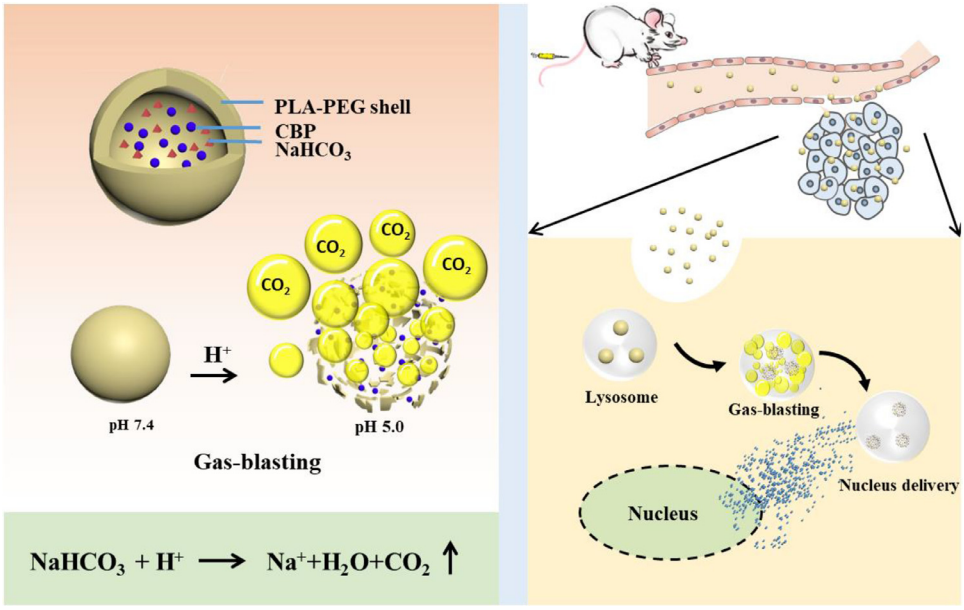

Scheme 1 – Design of CBP/SB-NC. The scheme shows the delivery mechanism of gas-blasting nanocapsules for accelerating CBP release and nucleus delivery. H^+ that infiltrated the CBP/SB-NC from the acidic organelles reacted with the $NaHCO_3$ therein, forming CO_2 bubbles. The evolution of CO_2 bubbles triggered the bursting of the shell by increasing the internal pressure, which can accelerate CBP release and nucleus delivery.

2.2. *Cell lines and animals*

Human prostate cancer cells (PC3) and mouse prostate cancer cells (RM-1) were purchased from Chinese Academy of Sciences (China). Both cell lines were cultured in RPMI-1640 medium at 37 °C in an environment containing 5% CO_2. The RPMI-1640 medium was supplemented with 10% FBS, 1% penicillin and 1% streptomycin. Male C57BL/6 (weight: 18–22 g) mice were supplied by SPF (Beijing) Biotechnology Co, Ltd. All experiments were carried out in accordance with the Animal Management Rules of the Ministry of Health of the People's Republic of China (document number 55, 2001) and the Animal Experiment Ethics Review of Shandong University (Approval No.18002).

2.3. *Preparation of CBP/SB-NC*

The preparation of CBP/SB-NC was prepared by w/o/w emulsification solvent evaporation [28]. CBP (15 mg/ml) and $NaHCO_3$ were dissolved in ddH_2O. PLA-PEG (10 mg) and span 80 (5 µl) were dissolved in 1 ml dichloromethane. Then 125 µl aqueous phase was added into the dichloromethane solution and sheared for 60 s at 20,000 rpm in ice bath. The obtained W/O emulsion were added dropwise into the 1.25 ml 1% PVA solution and sheared for 60 s at 20,000 rpm in ice bath to form CBP/SB-NC, then stir the CBP/SB-NC and volatilize the dichloromethane.

2.4. *Characterization of CBP/SB-NC*

Particle size, zeta potential and polydispersity index (PDI) of the CBP/SB-NC were measured using a Malvern Zeta Sizer Nano-ZS instrument (Malvern Instruments Ltd, UK.) at 25 °C. The mean particle size, PDI and zeta potential were evaluated in triplicate. The morphology of CBP/SB-NC was visualized by transmission electronic microscopy (TEM) (Hitachi, Japan). A drop of CBP/SB-NC was deposited on a copper grid, and then stained with one drop of phosphotungstic acid (2%, w/v).

The encapsulation efficiency of CBP was measured. The unencapsulated CBP was removed by centrifuging for 30 min at 12,500 rpm using an ultrafiltration centrifuge tube (MWCO = 3000 Da). The filtrates were collected and combined from the outer centrifuge tube to obtain separated unencapsulated CBP. A quantitative determination of unencapsulated CBP was made at 229 nm by using an HPLC with a 5 µm C_{18} column (4.6 mm × 250 mm) at room temperature. The mobile phase was constitutive of methanol-H_2O buffer (5:95, v/v). The samples were directly injected (20 µl) into the HPLC system without further treatment. The flow rate was 1.0 ml/min. The calibration curve of the peak area (A) *versus* CBP concentration (C) was $A = 10.261C + 3.630$ ($r = 0.99998$) over a range of standard CBP concentration between 2.5 and 80 µg/ml. The accuracy, recovery, precision, limit of detection and quantification were in accordance with methodological requirements. The encapsulation efficacy (EE%) and drug-loading efficacy (DL%) of CBP/SB-NC was calculated using the following equation:

$$EE\% = \frac{W_{\text{loaded drug}}}{W_{\text{total drug}}} \times 100$$

$$DL\% = \frac{W_{\text{loaded drug}}}{W_{\text{nanocapsules}}} \times 100$$

2.5. Storage stability

CBP/SB-NC was prepared and stored at 4 ± 2 °C. The changed particle sizes were recorded about 7 d as the evaluation index. All measurements were represented as mean ± SD ($n = 3$).

2.6. In vitro release

In order to investigate the effect of the concentration of $NaHCO_3$ on the pH responsive release, CBP-NC, CBP/$SB_{2.5}$-NC (2.5 mg/ml $NaHCO_3$), CBP/SB_5-NC (5 mg/ml $NaHCO_3$), CBP/SB_{10}-NC (10 mg/ml $NaHCO_3$) were prepared. *In vitro* release of CBP from the CBP/SB-NC was investigated by the dialysis method [32]. Briefly, each dialysis bag (3500 Da) containing 1 ml samples of CBP/SB-NC was incubated with 10 ml PBS (pH 7.4, 6.5, 5.0) as release medium at 37 °C with stirring at 100 rpm. At the predetermined time intervals, the release medium was take out and replaced with fresh medium. The cumulative amounts of CBP in the release medium were calculated by HPLC. All measurements were carried out in triplicate.

2.7. Gas-blasting evaluation

PBS (pH 7.4, 6.5, 5.0) was selected for the preliminary evaluation of the pH-sensitive gas-blasting explosion of the CBP/SB_5-NC. CBP/SB_5-NC was prepared and diluted with PBS (5 times) and incubation at 37 °C for 1, 2, 4 h. The TEM was selected to observe the changes of morphology. To further quantify the capability of pH-sensitive gas-blasting explosion of CBP/SB_5-NC, the change of the concentration of $H^+$was tested after CBP/SB_5-NC adjusted to pH 7.4, 6.5, 5.0 by HCl.

2.8. Cellular uptake of CBP/SB-NC

Fluorescein isothiocyanate (FITC) was selected as the tracer agent to label the CBP/SB-NC. Labeled nanocapsules were prepared by w/o/w emulsification solvent evaporation. RM-1 cells were seeded into 12-well plates and cultured overnight. The free FITC, FITC loaded nanocapsules (FITC-NC) and FITC and $NaHCO_3$ co-loaded nanocapsules (FITC/SB_5-NC) were added to the cells at the final concentrations of 50 μg/ml for FITC and incubated with the cells for 0.5, 1, 2 and 4 h. Subsequently, the cells were washed with cold PBS and then fixed with 4% paraformaldehyde. Cellular uptake of the FITC loaded nanocapsules was imaged by fluorescence microscope. In terms of the quantification of the cellular uptake efficiency, RM-1 cells were incubated with FITC labeled nanocapsules (5 μg/ml). The cells were washed and suspended in 200 μl of PBS, and cellular uptake was evaluated by a flow cytometer (CytoFLEX S, Beckman Coulter, USA).

2.9. PH-triggered rapid nucleus delivery

There is no evidence demonstrating that free FITC can enter the nucleus, however, DOX was demonstrated that had great capability of nucleus delivery. Meanwhile, DOX have red fluorescence which was easily for detection. So DOX was selected as model drug to evaluate whether the existence of $NaHCO_3$ can promote pH-triggered rapid nucleus delivery. DOX loaded nanocapsules were prepared by w/o/w emulsification solvent evaporation using the method in "2.3.Preparation of CBP/SB-NC" and the concentrations were tested. RM-1 cells were seeded in 12-well plates (2×10^5 cells per well) and cultured overnight. The free DOX, DOX loaded nanocapsules (DOX-NC), and DOX and $NaHCO_3$ co-loaded nanocapsules (DOX/SB_5-NC) were added to the cells at the final concentrations of 4 μg/ml for DOX and incubated with the cells for 0.25 and 0.5 h. Subsequently, the cells were washed with cold PBS and then fixed with 4% paraformaldehyde. The pH-triggered rapid nucleus delivery of nanocapsules was visualized using the fluorescence microscopy.

2.10. Pt-DNA adduct determination

Nuclear DNA was an important molecular target for CBP [10–12]. To further evaluate whether the existence of $NaHCO_3$ can promote pH-triggered rapid nucleus location, the relative quantity of adduct both platinum of DNA (Pt-DNA) was further tested to make verifications with pH-triggered rapid nucleus delivery. For Pt-DNA analysis, 2×10^6 RM-1 cells were seeded on 60 mm^2 dishes. 60 μg/ml CBP solutions, CBP-NC and CBP/SB_5-NC were added to the plates and incubated for 24 h, the cells were washed with cold PBS. Subsequently, the DNA was extracted using Nuclei EZ Prep Ki and diluted to 2 ml. The concentration of Pt was evaluated by ICP-MS.

2.11. In vivo NIRF imaging

Real-time near infra-red fluorophore (NIRF) imaging was selected to observe the biodistribution of the drugs [32]. CBP was replaced by a near infrared fluorophore dye (DiR) in the formulation. DiR loaded nanocapsules (DiR-NC) and DiR and $NaHCO_3$ co-loaded nanocapsules (DiR/SB_5-NC) were prepared by w/o/w emulsification solvent evaporation, and the final concentration of DiR was 50 μg/ml. The free DiR was dissolved in methanol (5 mg/ml) and then diluted to 50 μg/ml. Male RM-1 bearing C57BL/6 model was used for NIRF imaging. When the tumor grew to about 200–300 mm^3, mice were iv-injected with free DiR, DiR-NC and DiR/SB_5-NC (0.1 ml). After 2, 4, 8, 12 and 24 h, the mice were anesthetized injection of 10% chloral hydrate (i.p.) and observed. Afterwards, the mice were sacrificed and tumors and major organs were excised for *in vitro* imaging. The real-time NIRF images were tested using a real-time NIRF detector (Caliper Life Sciences, USA) at appropriate wavelengths (excitation wavelength of 745 nm, emission wavelength of 835 nm).

2.12. In vitro cytotoxicity assay

The cytotoxicity assay of CBP/SB-NC at different concentration of CBP was assessed on PC3 cells and RM-1 cells by standard MTT assay [22,33]. The PC3 cells and RM-1 cells (5×10^3/well) were seeded separately into 96-well plates per 150 μl per well. The cells were cultured overnight. 50 μl of the culture medium containing a series of different concentration of CBP/SB_5-NC, CBP-NC, CBP solution, SB-NC and blank nanocapsules (Blank-NC) were added to the cells. Each concentration was repeated three incubated pores. After 48 h of incubation, each well was added 20 μl of MTT solution

Table 1 – Characterization of CBP/SB-NC formulations ($n = 3$).

	Particle size (nm)	PDI	Zeta potential (mV)	EE (%)	DL (%)
CBP-NC	88 ± 11	0.211 ± 0.086	−11 ± 0.5	74.6 ± 1.3	14.9 ± 0.3
CBP/$SB_{2.5}$-NC	144 ± 10	0.313 ± 0.152	−12 ± 1.2	75.7 ± 1.9	14.7 ± 0.4
CBP/SB_5-NC	124 ± 18	0.251 ± 0.110	−12 ± 0.3	73.6 ± 2.4	13.8 ± 0.5
CBP/SB_{10}-NC	129 ± 19	0.303 ± 0.081	−13 ± 2.2	67.4 ± 5.5	14.5 ± 1.2

(5 mg/ml) and cultured for another 4 h at 37 °C. Then the medium was removed and 200 µl of DMSO was added per well. Cell culture medium without cells was applied as blank and cells without any treatment were served as control. The absorbance of DMSO solution was measured at 570 nm using a microplate reader (Elx800, BioTek, USA). Cell viability was calculated as follows:

$$\text{Cell Viability (\%)} = \frac{A_{sample} - A_{blank}}{A_{control} - A_{blank}} \times 100\%$$

Where A_{sample}, A_{blank} and $A_{control}$ represented the absorbance of cells treated with formulations, blank group and cells untreated group, respectively. All measurements were carried out in triplicate.

2.13. *In vivo anti-tumor activity*

RM-1 bearing male C57BL/6 mice was used to evaluate the *in vivo* anti-tumor efficacy of CBP/SB-NC [34]. The mice were hypodermically injected with 0.1 ml of cell suspension containing 1×10^6 RM-1 cells. After 8 d, the mice were randomly divided into 4 groups (6 mice per group): (1) normal saline (NS) (2) CBP solution (3) CBP-NC (4) CBP/SB_5-NC. Subsequently, the mice were treated with NS, CBP solution, CBP-NC and CBP/SB_5-NC by intravenous injection once 3 d (10 mg/kg). The tumor volumes and the body weights were measured every 2 d. Fifteen days later, the mice were sacrificed and tumors were taken out and photographed. The tumor volume (V) was calculated as follows:

$$V = \frac{W^2(\text{width}) \times L(\text{length})}{2}$$

2.14. *Hemolysis assay*

Red blood cells (RBCs) were diluted into 2% (v/v) cell suspension with NS. Then the RBCs suspension incubated with CBP/SB_5-NC at a CBP final concentration of 10, 20, 40, 60 and 80 µg/ml at 37 ± 0.5 °C for 3 h. NS was regarded as a negative control and distilled water was regarded as a positive control. Finally, the absorbance of hemoglobin was determined after centrifuging using a UV–vis spectrophotometer at 576 nm. The hemolysis percentage of the RBCs was calculated as follows:

$$\text{HR (\%)} = \frac{A_{sample} - A_{negative}}{A_{posotive} - A_{negative}} \times 100\%$$

Where A_{sample}, $A_{negative}$ *and* $A_{positive}$ represent the absorbance of the sample, negative control and positive control, respectively.

2.15. *Histopathological study*

Male C57BL/6 mice (18–22 g) were injected with control, CBP solution, CBP/SB_5-NC, CBP-NC by intravenous injection once 3 d. Fifteen days later, the mice were sacrificed and tumors and major organs were excised and fixed with 4% formaldehyde. Then, the major organs were embedded in paraffin and stained with H&E for histological examination. The tumor tissue was fixed with 4% formaldehyde and embedded in paraffin. Then it was stained with Ki-67 for histological examination.

2.16. *Statistics analysis*

Statistical differences were analyzed with Student's *t*-test. Differences were considered to be statistically significant when the $P < 0.05$. All data were reported as the mean ± SD.

3. Results and discussion

3.1. *Preparation and characterization of CBP/SB-NC*

CBP and $NaHCO_3$ co-loaded nanocapsules (CBP-NC, CBP/$SB_{2.5}$-NC, CBP/SB_5-NC, CBP/SB_{10}-NC) were prepared. Mean particle size, zeta potential and morphologies of CBP/SB-NC with different concentration of $NaHCO_3$ were shown in Fig. 1A. In addition, the characterizations of CBP/SB-NC formulations were summarized in Table 1. The results showed that the encapsulation of additional $NaHCO_3$ cause the increase of the size of CBP nanocapsules, but did not showed significantly change in zeta potential, encapsulation efficacy and drug loading. CBP/SB-NC with different concentration of $NaHCO_3$ possessed uniform particle size, high drug loading and entrapment efficiency. Transmission electron microscope observation showed that the morphology of CBP/SB-NCs were vesicle-like spherical shape.

The storage stability of CBP/SB_5-NC was evaluated by the changed particle sizes using DLS at 4 ± 2 °C (Fig. 1B). The results showed a minimal change of CBP/SB_5-NC, indicating that the CBP/SB_5-NC were stable in 7 d. Diluted CBP/SB_5-NC (Fig. 1C) could observe a red light path in the vertical direction when the formulation was irradiated with laser, indicating that CBP/SB_5-NC was nano-colloidal dispersion system.

3.2. *Gas-blasting evaluation and in vitro drug release*

CBP/SB_5-NC was prepared and diluted with PBS (5 times) and incubation at 37 °C for 1, 2 and 4 h. As shown in Fig. 2A,

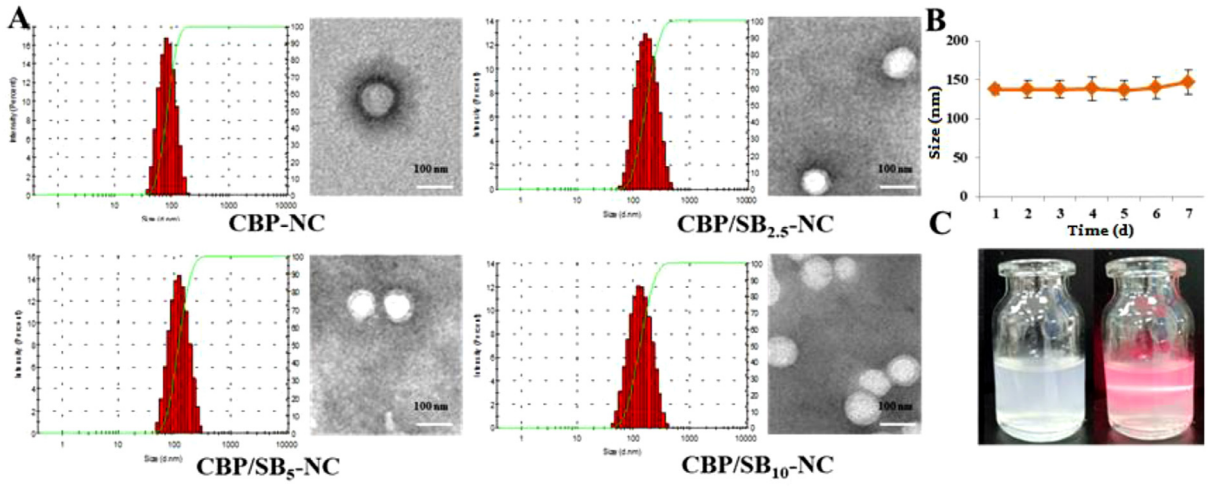

Fig. 1 – Characterizations of CBP/SB-NC. (A) Size distribution and morphology of CBP-NC, CBP/$SB_{2.5}$-NC, CBP/SB_5-NC and CBP/SB_{10}-NC (B) Storage stability of CBP/SB_5-NC. (C) Appearance of CBP/SB-NC.

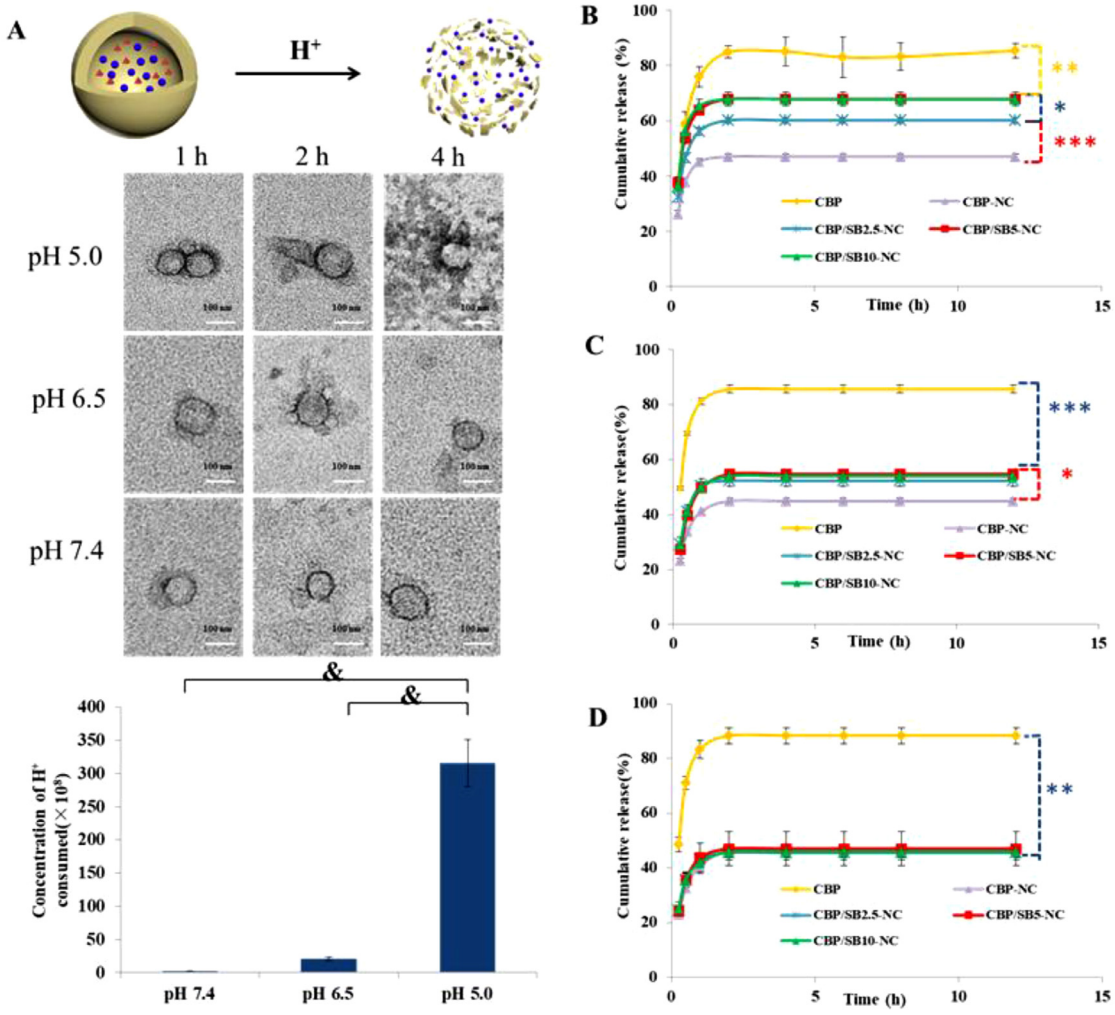

Fig. 2 – CBP/SB-NCs achieve lysosome pH-responsive CO_2 generation, leading to CBP blasting release. (A) Morphology of CBP/SB_5-NC incubated at 37 °C in pH 7.4, 6.5, 5.0. Concentration of H^+ consumed after CBP/SB_5-NC incubated for 4 h in pH 7.4, 6.5, 5.0. (B) *In vitro* release of CBP/SB-NC in pH 5.0; (C) pH 6.5; (D) pH 7.4. (Notes: & $P < 0.001$, * $P < 0.05$, ** $P < 0.01$, *** $P < 0.001$).

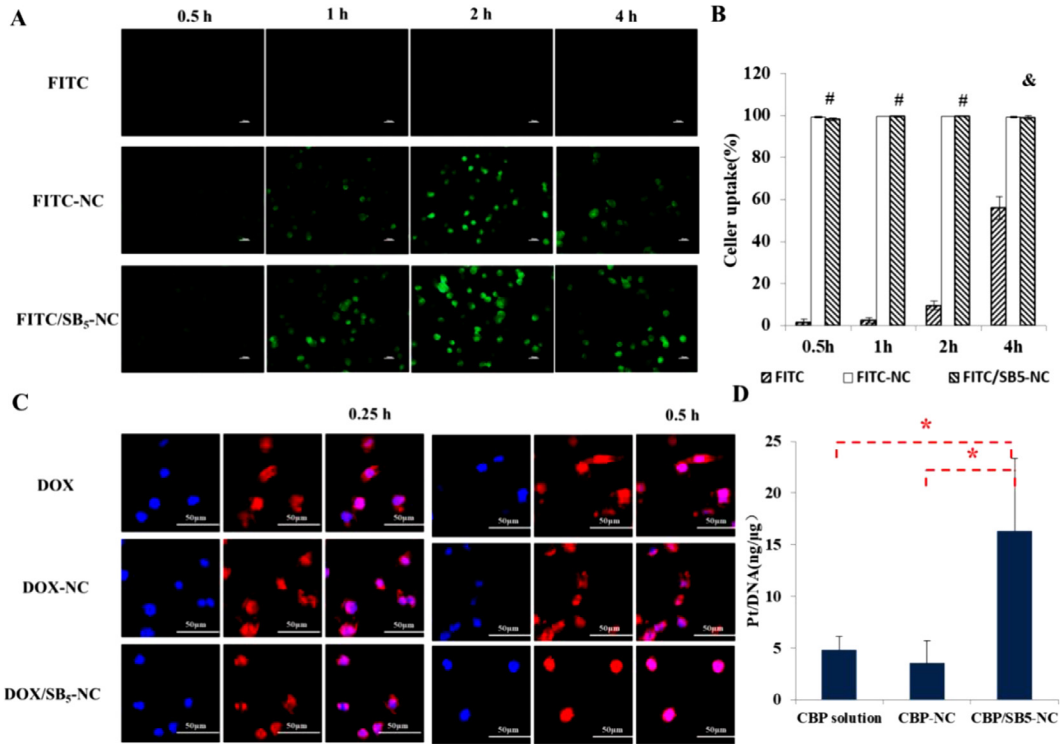

Fig. 3 – CBP/SB_5-NC can enhance cellular uptake and simultaneously achieve rapid co-localization with the nucleus. (A) Inverted fluorescence microscopy images (FITC: 50 μg/ml) of cellular uptake on RM-1cells (40 ×); (B) Flow cytometer analysis of RM-1 cells. Quantification data of cellular uptake in RM-1cells (FITC: 5 μg/ml); data are provided as means ± SD ($n = 3$). (C) Inverted fluorescence microscopy images about nucleus location of RM-1 cells incubated for 0.25 h and 0.5 h with DOX, DOX-NC and DOX/SB_5-NC. (D) Pt-DNA binding in RM-1 cells after treatment with CBP solution or an equivalent Pt dose of CBP-NC and CBP/SB_5-NC. Data are provided as means ± SD ($n = 3$). (Notes: & $P < 0.01$, #$P < 0.001$ (FITC-NC or FITC/SB_5-NC *vs.* FITC at the same time), *$P < 0.05$).

the shell of CBP/SB_5-NC was complete in pH 6.5 and 7.4, but the capsule shell of CBP/SB_5-NC was cracked in pH 5.0 after incubation for 4 h. The change of the concentration of $H^+$of CBP/SB_5-NC after incubation for 4 h in pH 5.0, 6.5 and 7.4 showed that CBP/SB_5-NC consumed more $NaHCO_3$ in pH 5.0, which was consistent with the microscopy images. The results of release behavior indicted that CBP-NC, CBP/$SB_{2.5}$-NC, CBP/SB_5-NC and CBP/SB_{10}-NC all had no significant difference in pH 7.4 (Fig. 2D). The cumulative release of CBP/$SB_{2.5}$-NC, CBP/SB_5-NC and CBP/SB_{10}-NC for 12 h in pH 6.5 was 52.29%, 54.75% and 54.05%, respectively. While, there was no significant difference of CBP/SB-NC with a series of different concentration of $NaHCO_3$ in pH 6.5 (Fig. 2C). As shown in Fig. 2B, the cumulative release of CBP/$SB_{2.5}$-NC, CBP/SB_5-NC and CBP/SB_{10}-NC for 12 h in pH 5.0 was 60.15%, 67.80% and 67.83%, respectively, which was higher than CBP-NC (47.05%), indicating that the gas-blasting strategy can achieve pH-sensitive release. Beyond that, the cumulative CBP release of CBP/SB_5-NC for 12 h was higher than that of CBP/$SB_{2.5}$-NC ($P < 0.05$), but there was no difference between CBP/SB_5-NC and CBP/SB_{10}-NC in pH 5.0 ($P > 0.05$). Therefore, the optimal concentration of $NaHCO_3$ was 5 mg/ml, and the pH-triggered blasting of CBP/SB_5-NC was observed. These results indicated that CO_2 was produced by the reaction of $NaHCO_3$ in the CBP/SB_5-NC with H^+ under lysosome acid environment (pH 5.0). The production of CO_2 bubbles triggered the blasting of the shell by increasing the internal pressure, which can accelerate CBP lysosome release to cytoplasm.

3.3. *Cellular uptake of CBP/SB-NC*

The cellular uptake of free FITC, FITC-NC and FITC/SB_5-NC with an equivalent concentration of FITC (50 μg/ml) was conducted on RM-1 cells by fluorescence microscopy after 0.5, 1, 2 and 4 h incubation. The images (Fig. 3A) showed that the fluorescence of FITC-NC and FITC/SB_5-NC was higher than free FITC. The internalization of nanocapsules was presented by the cellular uptake rate calculated from flow cytometer data (Fig. 3B), which showed the same results with the images. These results indicated that the FITC-NC and FITC/SB_5-NC had effective cellular uptake ability on RM-1 cells, which was beneficial for improving the anti-tumor efficacy.

3.4. *PH-triggered rapid nucleus delivery*

The accelerated drug lysosome release was beneficial for nucleus delivery of CBP, enhanced binding efficiency of CBP with DNA, thus improving the anti-tumor effect of CBP. In order to evaluate whether the released CBP could enter

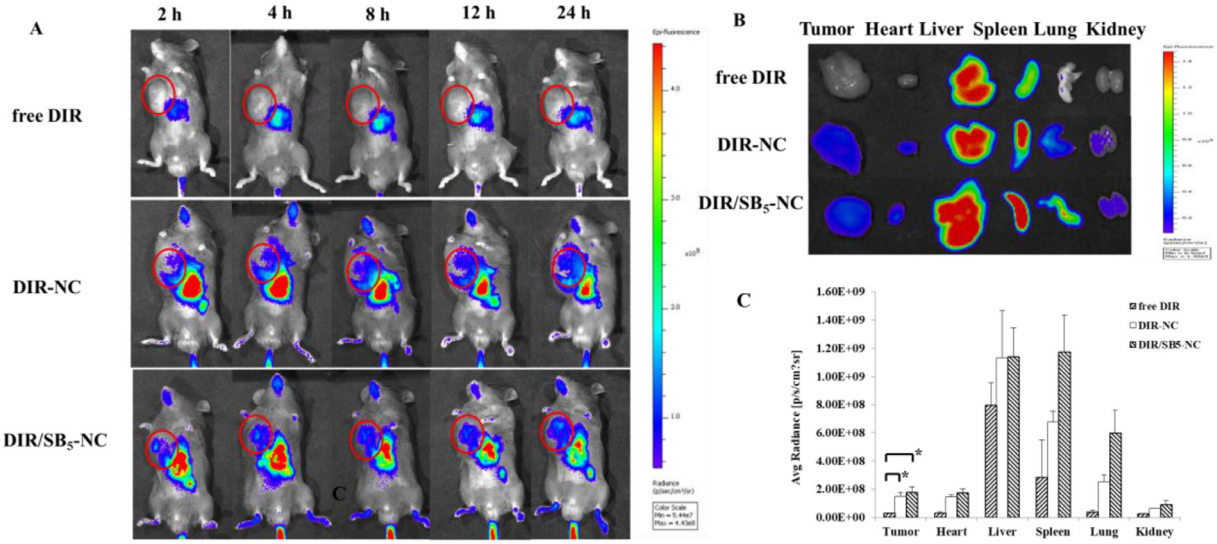

Fig. 4 – CBP/SB_5-NC display enhanced tumor accumulation. (A) *In vivo* imaging of mice of tumor-bearing mice post i.v. administration with free DiR, DiR-NC, DiR/SB_5-NC at different time points. Tumors were marked with red circles; (B) *In vitro* imaging of the main organs and tumors in free DiR, DiR-NC and DiR/SB_5-NC groups after the mice were anatomized at 24 h post administration; (C) The fluorescent intensity in the main organs and tumors based on the *in vitro* results. (Notes: *$P < 0.05$).

the nucleus and bind with DNA, the nucleus delivery was further tested by the co-localization in RM-1 cells. DOX which have nucleus entering capability and red fluorescence was selected model drug. Cells incubated with DOX, DOX-NC and DOX/SB_5-NC, and the nucleus delivery was indicated by purple fluorescence due to merging of red (DOX) and blue (DAPI) fluorescence (Fig. 3C). Purple fluorescence boosted up with the increase of incubation time, demonstrating that more DOX was delivered into the nucleus of RM-1 cells. Moreover, as shown in Fig. 3C, the existence of red fluorescence around the nucleus showed that DOX was still exist in the around of nucleus of DOX, DOX-NC and DOX/SB_5-NC after 0.25 h incubation. While, after 0.5 h incubation, DOX/SB_5-NC could be clearly found that the DOX was completely entering the nucleus, but DOX was still exist in the around of nucleus of DOX and DOX-NC group, demonstrating that more DOX was delivered into the nucleus of RM-1 cells.

3.5. *Pt-DNA adduct determination*

As shown in the Fig. 3D, the CBP/SB_5-NC possessed higher Pt-DNA adduct efficiency, which was 3-fold higher than CBP solution and 4-fold higher than CBP-NC. These results showed that CBP/SB_5-NC could improve the Pt-DNA adduct efficiency compared to CBP solution ($P < 0.05$) and CBP-NC ($P < 0.05$).

3.6. *In vivo NIRF imaging*

NIRF imaging was applied to observe the biodistribution of the CBP/SB-NC *in vivo*. As shown in Fig. 4A, free DiR could scarcely observe the DiR signal in the tumor site. By contrast, DiR-NC and DiR/SB_5-NC showed stronger DiR signals in the tumor site for 24 h, demonstrating that DiR-NC and DiR/SB_5-NC could enhance payload accumulation in the tumor sites. To accurately indicate the biodistribution of CBP-NC and CBP/SB_5-NC, the mice were sacrificed after 24 h, and the tumor and major organs were excised. The *in vitro* image exhibited DiR-NC and DiR/SB_5-NC were obviously increased in the tumor site (Fig. 4B). Moreover, the average fluorescence intensity of different organs at 24 h was calculated (Fig. 4C). Nearly 1.50×10^8 and 1.76×10^8 dye signal were observed in tumor site in DiR-NC and DiR/SB_5-NC group, which were higher than that in free DiR group ($P < 0.05$). These results demonstrated that DiR/SB_5-NC could effectively increase drug accumulation at tumor site and lower the severely side effects, thus improving the anti-tumor efficacy.

3.7. *In vitro cytotoxicity assay*

In vitro cytotoxicity assay of CBP/SB-NC was assessed on PC3 cells and RM-1 cells by MTT method. As shown in Fig. 5A and 5B, cell viabilities of Blank-NC group and SB-NC group were higher than ~80% at all tested concentration on RM-1 and PC3 cells, suggesting low toxicity of Blank-NC and SB-NC. Moreover, CBP/SB_5-NC showed similar cytotoxicity to the CBP solution. The CBP-NC showed less cytotoxicity than CBP solution and CBP/SB_5-NC, which could be contribute to the lower amount of released CBP than CBP solution and CBP/SB_5-NC in the pH responsive release experiments. The half maximal inhibitory concentration (IC_{50}) was shown in Table 2. The IC_{50} values of CBP/SB_5-NC were 22.71 μg/ml on RM-1 cell lines, which was similar to the CBP solution ($P > 0.05$) and significantly lower than that of CBP-NC group ($P < 0.05$). And the IC_{50} values of CBP/SB_5-NC was 19.83 μg/ml on PC3 cell lines (Fig. 5B), which were lower than that of CBP solution ($P < 0.01$) and CBP-NC group ($P < 0.05$). These results showed CBP/SB_5-NC exhibited better anti-tumor activity compared with CBP solution on the two cell lines.

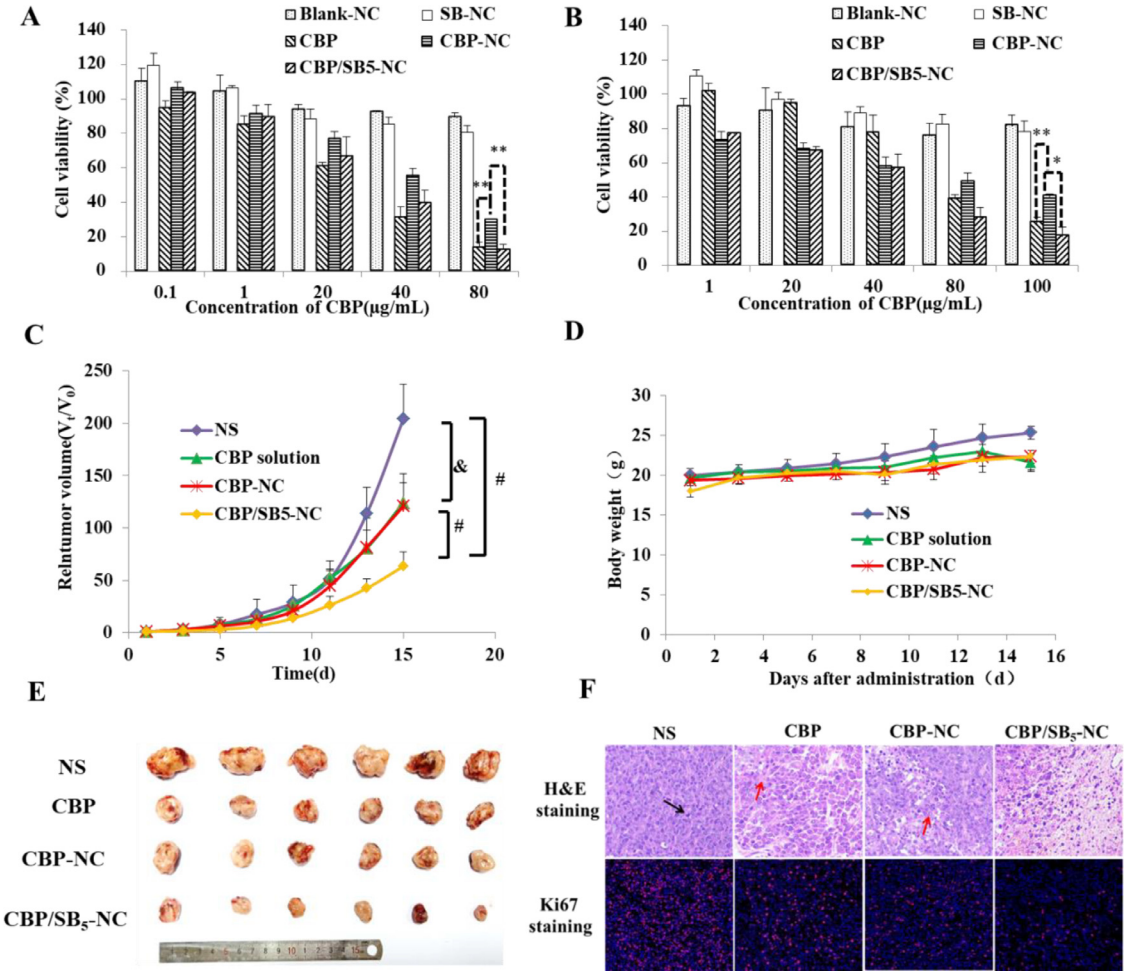

Fig. 5 – CBP/SB_5-NC display remarkable antitumor effect *in vitro* and *in vivo*. (A) *In vitro* cytotoxicity on RM-1 cell and (B) PC3 cell; (C) *In vivo* antitumor efficacy in RM-1 tumor-bearing mice injected with NS, CBP solution, CBP-NC and CBP/SB_5-NC. Tumor volume change in different treatment groups ($n = 6$); (D) Body weight changes post administration; (E) A photograph of tumors excised from each treatment group; (F) The microphotographs of H&E and Ki-67 staining assay of tumor tissues in different groups(400 x). (Notes: *$P < 0.05$, **$P < 0.01$, &$P < 0.01$, #$P < 0.001$).

Table 2 – IC_{50} values of different groups against RM-1 and PC3 cells.

IC_{50}	CBP	CBP-NC	CBP/SB_5-NC
RM-1	13.17 ± 0.94	36.50 ± 2.15***	22.71 ± 4.12#
PC3	73.18 ± 7.83	76.63 ± 16.15	19.83 ± 3.82#,**

Notes:
# $P < 0.05$ (CBP/SB_5-NC *vs.* CBP-NC).
** $P < 0.01$, (CBP/SB_5-NC *vs.* CBP).
*** $P < 0.001$, (CBP-NC *vs.* CBP).

3.8. *In vivo anti-tumor activity*

The anti-tumor efficacy of CBP/SB-NC was evaluated on the RM-1 bearing male C57BL/6 mice model. As shown in Fig. 5, CBP solution, CBP-NC and CBP/SB_5-NC displayed remarkable reduction of relative tumor volume (Fig. 5C) during the administration period compared with NS group ($P < 0.01$). Of note, CBP solution and CBP-NC groups showed similar anti-tumor activity ($P > 0.05$). Moreover, CBP/SB_5-NC showed better anti-tumor efficacy than CBP solution and CBP-NC ($P < 0.001$).

The results of photographs of tumors (Fig. 5E) were corresponding with the tumor volume. CBP/SB_5-NC showed superior anti-tumor activity compared with CBP solution and CBP-NC groups ($P < 0.001$). The body weights were used to evaluate the primary safety of the formulations. As shown in Fig. 5D, there was no severe body weight loss observed in all groups.

H&E and Ki-67 staining of tumor tissues were carried out to further verify the enhanced anti-tumor efficacy of CBP/SB-NC (Fig. 5F). The results of H&E staining showed that the structure of tumor cells was complete and nearly no necrosis was found in NS group. Moreover, a small amount of nuclear mitosis could be observed (black arrows). The tumor cells necrosis and nuclear dissolving of necrotic tumor could be observed in CBP solution and CBP-NC groups (red arrows). In CBP/SB_5-

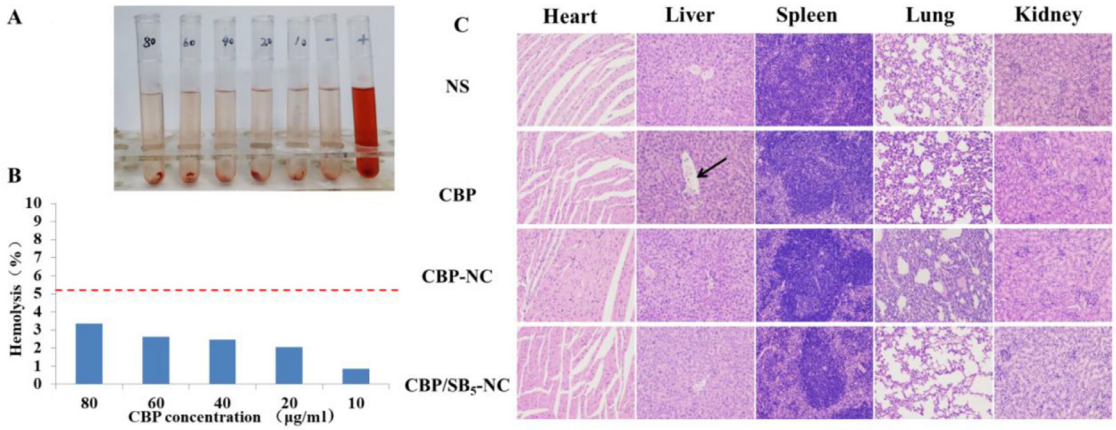

Fig. 6 – CBP/SB_5-NC show unregulated safety *in vitro* and *in vivo*. (A) Photograph of hemolysis assay observed by naked eyes of CBP/SB_5-NC at different concentrations; (B) Hemolysis percentage of RBCs and the image after RBCs suspension was incubated with CBP/SB_5-NC, within a CBP range of 10–80 μg/ml for 3 h. Distilled water (+) and NS (-) were used as positive and negative control, respectively. (C) Representative microscopy photographs of H&E stained histological sections of main organs from male C57BL/6 mice after treatment with NS, CBP solution, CBP-NC and CBP/SB_5-NC (200 ×).

NC group, large area necrosis and dissolution of tumor cells were found in the tumor tissue, which further confirmed that CBP/SB_5-NC had the most prominent tumor suppressible effect *in vivo*.

The results of Ki-67 staining showed that a large number of red positive cells were observed in tumor tissues of NS group, indicating that the proliferation of tumor cells was much strong in NS group. While the number of red positive cells in CBP solution and CBP-NC groups obviously decreased, demonstrating that the proliferation of tumor cells was suppressed after administration of CBP solution and CBP-NC. The red tumor cells in CBP/SB_5-NC treated group were further reduced, which manifested that CBP/SB_5-NC had the strongest inhibitory effect on the proliferation of tumor cells.

All of the results proved that CBP/SB_5-NC could enhance anti-tumor activity *in vivo* for prostate cancer therapy.

3.9. *Hemolysis assay*

As shown in Fig. 6A and 6B, in the range of 10–80 μg/ml of CBP/SB_5-NC, no hemolysis and erythrocyte aggregation phenomenon were observed in the groups and the hemolytic activity of CBP/SB_5-NC was negligible (< 5%). The results suggested that CBP/SB_5-NC exhibited good hemocompatibility and was appropriate for intravenous administration.

3.10. *Histopathological study*

To assess the safety and histocompatibility of CBP/SB-NC, histological observation was employed after administration of CBP/SB-NC. As shown in Fig. 6C, no visible organ damage of the CBP/SB_5-NC group was observed. While in CBP solution group, an abnormal morphology was observed in the livers. As marked by the arrow, vacuolar cell and necrosis of liver could be observed. This result indicated that CBP/SB_5-NC can reduce the toxicity of CBP *in vivo* under our experimental conditions.

4. Conclusion

In the study, CBP/SB-NC was prepared for accelerating CBP lysosome release and nucleus delivery. CBP/SB-NC exhibited uniform size distribution and high drug loading ability. The pH-sensitive gas-blasting release property was observed in drug release studies. Moreover, CBP/SB-NC showed high tumor accumulation, improved cellular uptake and drug-nucleus co-location, which contributed to superior anti-tumor efficacy *in vivo*. CBP/SB-NC was a potential formulation to enhance prostate cancer therapy. Our results demonstrated that gas-blasting release strategy provided a promising way for facilitate nucleus delivery and tumor treatment for CBP.

Conflicts of interest

The authors report no conflicts of interest. The authors alone are responsible for the content and writing of this article.

Acknowledgments

This work was supported by a grant from the National Natural Science Foundation of China (Nos. 81773652 and 81974498) and the Young Scholar Program of Shandong University (2017WLJH40). We thank Translational Medicine Core Facility of Shandong University for consultation and instrument availability that supported this work.

REFERENCES

[1] Bray F, Ferlay J, Soerjomataram I, Siegel RL, Torre LA, Jemal A. Global cancer statistics 2018: GLOBOCAN estimates of incidence and mortality worldwide for 36 cancers in 185 countries. CA Cancer J Clin 2018;68(6):394–424.

[2] Meijer GA. GLOBOCAN 1: cancer incidence and mortality worldwide. J Clin Pathol 2000;53(2):164.
[3] Cha E, Fong L. Immunotherapy for prostate cancer: biology and therapeutic approaches. J Clin Oncol 2011;29(27):3677–85.
[4] Tosco L, Briganti A, D'amico AV, Eastham J, Eisenberger M, Gleave M, et al. Systematic review of systemic therapies and therapeutic combinations with local treatments for high-risk localized prostate cancer. Eur Urol 2019;75(1):44–60.
[5] He C, Tang Z, Tian H, Chen X. Co-delivery of chemotherapeutics and proteins for synergistic therapy. Adv Drug Deliv Rev 2016;98:64–76.
[6] Barve A, Jin W, Cheng K. Prostate cancer relevant antigens and enzymes for targeted drug delivery. J Control Release 2014;187:118–32.
[7] Chen J, Zhang W, Zhang M, Guo Z, Wang H, He M, et al. Mn(II) mediated degradation of artemisinin based on Fe_3O_4@$MnSiO_3$-FA nanospheres for cancer therapy *in vivo*. Nanoscale 2015;7(29):12542–51.
[8] Hager S, Ackermann CJ, Joerger M, Gillessen S, Omlin A. Antitumour activity of platinum compounds in advanced prostate cancer - a systematic literature review. Ann Oncol 2016;27(6):975–84.
[9] Omlin A, Gillessen S. When and how to use carboplatin in metastatic castration-resistant prostate cancer? Eur J Cancer 2018;92:96–9.
[10] Browning RJ, Reardon PJT, Parhizkar M, Pedley RB, Edirisinghe M, Knowles JC, et al. Drug delivery strategies for platinum-based chemotherapy. ACS Nano 2017;11(9):8560–78.
[11] Kelland L. The resurgence of platinum-based cancer chemotherapy. Nat Rev Cancer 2007;7(8):573–84.
[12] Zhang M, Hagan CTT, Min Y, Foley H, Tian X, Yang F, et al. Nanoparticle co-delivery of wortmannin and cisplatin synergistically enhances chemoradiotherapy and reverses platinum resistance in ovarian cancer models. Biomaterials 2018;169:1–10.
[13] Aparicio AM, Harzstark AL, Corn PG, Wen S, Araujo JC, Tu SM, et al. Platinum-based chemotherapy for variant castrate-resistant prostate cancer. Clin Cancer Res 2013;19(13):3621–30.
[14] Borghaei H, Langer CJ, Gadgeel S, Papadimitrakopoulou VA, Patnaik A, Powell SF, et al. 24-Month overall survival from KEYNOTE-021 Cohort G: pemetrexed and carboplatin with or without pembrolizumab as first-line therapy for advanced nonsquamous non-small cell lung cancer. J Thorac Oncol 2019;14(1):124–9.
[15] Inui N. Antiemetic therapy for non-anthracycline and cyclophosphamide moderately emetogenic chemotherapy. Med Oncol 2017;34(5):77.
[16] Mcilwain H. Biochemistry and chemotherapy. Nature 1943;151(3827):270–3.
[17] Khatun Z, Nurunnabi M, Nafiujjaman M, Reeck GR, Khan HA, Cho KJ, et al. A hyaluronic acid nanogel for photo-chemo theranostics of lung cancer with simultaneous light-responsive controlled release of doxorubicin. Nanoscale 2015;7(24):10680–9.
[18] Maeda H. Macromolecular therapeutics in cancer treatment: the EPR effect and beyond. J Control Release 2012;164(2):138–44.
[19] Nichols J W, Bae YH. EPR: evidence and fallacy. J Control Release 2014;190:451–64.
[20] Markman JL, Rekechenetskiy A, Holler E, Ljubimova JY. Nanomedicine therapeutic approaches to overcome cancer drug resistance. Adv Drug Deliv Rev 2013;65(13–14):1866–79.
[21] Lin YJ, Huang CC, Wan WL, Chiang CH, Chang Y, Sung HW. Recent advances in CO_2 bubble-generating carrier systems for localized controlled release. Biomaterials 2017;133:154–64.
[22] Liang S, Han LQ, Mu WW, Jiang DD, Hou T, Yin XL, et al. Carboplatin-loaded SMNDs to reduce GSH-mediated platinum resistance for prostate cancer therapy. J Mater Chem B 2018;6:7004–14.
[23] Liao ZX, Chuang EY, Lin CC, Ho YC, Lin KJ, Cheng PY, et al. An AS1411 aptamer-conjugated liposomal system containing a bubble-generating agent for tumor-specific chemotherapy that overcomes multidrug resistance. J Control Release 2015;208:42–51.
[24] Chung MF, Chen K J, Liang HF, Liao ZX, Sung HW. A liposomal system capable of generating CO_2 bubbles to induce transient cavitation, lysosomal rupturing, and cell necrosis. Angew Chem 2012;51(40):10089–93.
[25] Chung MF, Chia WT, Liu HY, Hsiao CW, Hsiao HC, Yang CM, et al. Inflammation-induced drug release by using a pH-responsive gas-generating hollow-microsphere system for the treatment of osteomyelitis. Adv Healthc Mater 2014;3(11):1854–61.
[26] Jiang D, Zhang X, Yu D, Xiao Y, Wang T, Su Z, et al. Tumor-microenvironment relaxivity-changeable Gd-loaded poly(L-lysine)/carboxymethyl chitosan nanoparticles as cancer-recognizable magnetic resonance imaging contrast agents. J Biomed Nanotechnol 2017;13(3):243–54.
[27] Ke CJ, Lin YJ, Hu YC, Chiang WL, Chen KJ, Yang WC, et al. Multidrug release based on microneedle arrays filled with pH-responsive PLGA hollow microspheres. Biomaterials 2012;33(20):5156–65.
[28] Ke CJ, Chiang WL, Liao ZX, Chen HL, Lai PS, Sun JS, et al. Real-time visualization of pH-responsive PLGA hollow particles containing a gas-generating agent targeted for acidic organelles for overcoming multi-drug resistance. Biomaterials 2013;34(1):1–10.
[29] Yang L, Wen Z, Long Y, Huang N, Cheng Y, Zhao L, et al. A H^+-triggered bubble-generating nanosystem for killing cancer cells. Chem Commun 2016;52(72):10838–41.
[30] Liu J, Ma H, Wei T, Liang XJ. CO_2 gas induced drug release from pH-sensitive liposome to circumvent doxorubicin resistant cells. Chem Commun Camb 2012;48(40):4869–71.
[31] Casey J R, Grinstein S, Orlowski J. Sensors and regulators of intracellular pH. Nat Rev Mol Cell Biol 2010;11(1):50–61.
[32] Zhang B, Wang T, Yang S, Xiao Y, Song Y, Zhang N, et al. Development and evaluation of oxaliplatin and irinotecan co-loaded liposomes for enhanced colorectal cancer therapy. J Control Release 2016;238:10–21.
[33] Xia H, Luo X, Yin W. Inhibition of prostate cancer growth by immunization with a GM-CSF-modified mouse prostate cancer RM-1 cell vaccine in a novel murine model. Oncol Lett 2018;15(1):538–44.
[34] Zhao K, Li D, Xu W, Ding J, Jiang W, Li M, et al. Targeted hydroxyethyl starch prodrug for inhibiting the growth and metastasis of prostate cancer. Biomaterials 2017;116:82–94.